



HAL
open science

Embryonic zeolite-directed synthesis of ZSM-34 and SSZ-13 zeolites

Lingxue Tang, Kok-Giap Haw, Diandian Shi, Yuming Guo, Qianrong Fang,
Shilun Qiu, Valentin Valtchev

► **To cite this version:**

Lingxue Tang, Kok-Giap Haw, Diandian Shi, Yuming Guo, Qianrong Fang, et al.. Embryonic zeolite-directed synthesis of ZSM-34 and SSZ-13 zeolites. Green Carbon, In press, 10.1016/j.greenca.2024.04.002 . hal-04635870

HAL Id: hal-04635870

<https://hal.science/hal-04635870v1>

Submitted on 4 Jul 2024

HAL is a multi-disciplinary open access archive for the deposit and dissemination of scientific research documents, whether they are published or not. The documents may come from teaching and research institutions in France or abroad, or from public or private research centers.

L'archive ouverte pluridisciplinaire **HAL**, est destinée au dépôt et à la diffusion de documents scientifiques de niveau recherche, publiés ou non, émanant des établissements d'enseignement et de recherche français ou étrangers, des laboratoires publics ou privés.

Embryonic zeolite-directed synthesis of ZSM-34 and SSZ-13 zeolites

*Lingxue Tang,^{a,b} Kok-Giap Haw,^b Diandian Shi,^c Yuming Guo,^a Qianrong Fang,^b
Shilun Qiu,^b Valentin Valtchev,^{c,d*}*

^a School of Chemistry and Chemical Engineering, Henan Normal University,
Xinxiang 453007, PR China.

^b State Key Laboratory of Inorganic Synthesis and Preparative Chemistry, Jilin
University, Changchun 130012, China.

^c The ZeoMat Group, Qingdao Institute of Bioenergy and Bioprocess Technology,
Chinese Academy of Science, Laoshan District, CN-266101 Qingdao, China.

^d Normandie Univ, ENSICAEN, CNRS, Laboratoire Catalyse et Spectrochimie, 6
Marechal Juin, 14050 Caen, France.

E-mail : valentin.valtchev@ensicaen.fr

Abstract

The use of an organic structure-directing agent (OSDA) makes zeolite synthesis expensive and environmentally non-friendly. Seeded zeolite synthesis offers an environmentally benign alternative that avoids using an OSDA while providing a high

purity, crystallinity, and yield in the product. In this study, we report using embryonic zeolites (EZs) as efficient seeds to obtain industrially important zeolites such as ZSM-34 and SSZ-13 in an OSDA-free synthesis system. Our results showed that zeolites ZSM-34, SSZ-13 and LTL could be obtained depending on the Al/Si ratio in the synthesis system. The synthesis time was considerably shorter than other ZSM-34 and SSZ-13 syntheses methods reported in the literature, achieving more than 90% crystallinity. The physicochemical analysis showed that highly crystalline zeolites with characteristics similar to the OSDA synthesized counterparts were obtained. Furthermore, the EZs seeding approach is facile, low cost, and environmentally friendly, provided the synthesis is OSDA-free, in addition, the EZs seeds can be obtained under hydrothermal synthesis conditions. The method can be potentially applied to the synthesis of other zeolite types.

Keywords: Zeolite, OSDA-free, Embryonic zeolites, Seeded synthesis, Crystal growth kinetics

1.0 Introduction

Aluminosilicate zeolites are regarded as the industry's most important heterogeneous acid catalysts due to their well-defined micropores with excellent shape-selectivity, large surface area, high adsorption capacity, and high thermal and chemical stability [1-3]. Over the years, the number of new zeolite structures has been steadily increasing. Up to now, 256 zeolite framework types have been discovered

according to the structure database of the International Zeolite Association (IZA) [4]. The majority of zeolite syntheses needs to rely on an organic template as a structure-directing agent (OSDA) [5-9], but this method has disadvantages such as being non-environment friendly and expensive [10-14].

Important industrial materials such as ZSM-34 and SSZ-13 zeolites require the employment of an OSDA in their synthesis. Aluminosilicate zeolite ZSM-34 is an intergrown phase between offretite (OFF) and erionite (ERI) types [15,16] zeolite. The pore size (5.2 Å), and appropriate Al/Si ratio make ZSM-34 a suitable catalyst to convert methanol to olefins (C₂-C₅) [17-21]. ZSM-34 zeolite was initially synthesized in the presence of organic templates such as choline [(CH₃)₃NCH₂CH₂OH] and diamines of different lengths (NH₂C_nH_{2n}NH₂, n = 4, 6, 8, 10). The initial gel was subjected to long crystallization, usually not less than 25 days at 100 °C [22]. Some progress was made by Wu *et al.* and Yang *et al.*, who reported the first OSDA-free synthesis of zeolite ZSM-34 using zeolite L solution as seed. Unfortunately, the reaction time was relatively long (7 – 17 days) even after extensive optimization efforts [23,24]. Yang *et al.* reported that seeding with ZSM-34 can further decrease the reaction time to 2 hours. However, the yield (27%) was very low [25].

The framework of zeolite SSZ-13 (CHA-type) consists of an elliptical CHA cage (6.7 x 10 Å) connected by a three-dimensional pore system with 8-membered rings opening (3.8 x 3.8 Å). Besides the conventional synthesis from chemical reactants, the interzeolite conversion of FAU, Beta, LTL, LEV, USY, and cubic P was used to

obtain the low to high silica form of CHA-type zeolite [26-32]. Other approaches to synthesize SSZ-13 have also been reported [33-35]. Wang *et al.* recently synthesized nano-zeolite SSZ-13 in the presence of OSDA and embryonic zeolite solution as seeds [36].

In this paper, we investigated the effect of embryonic zeolites (EZs) as seeds in an OSDA-free synthesis of ZSM-34 and SSZ-13 zeolites. The goal is to shorten crystallization while obtaining high product yield and crystallinity. The ultimate goal of the study is to minimize the negative impact of zeolite production on the environment, particularly the release of CO₂ and NO_x in the atmosphere.

2.0 Experimental

2.1 Materials

The following reactants were used: potassium hydroxide (KOH 98%, Aladdin Chemistry), N,N,N-trimethyl-1-adamantammonium hydroxide (TMAD 35% aq., Aladdin Chemistry), tetraethyl orthosilicate (TEOS 98%, Sigma-Aldrich), aluminum powder (99.5%, Aladdin Chemistry), sodium nitrate (99.5%, Aladdin Chemistry), Ludox HS-40 (40 wt.% SiO₂, Sigma-Aldrich), aluminum sulfate octadecahydrate (Al₂(SO₄)₃·18H₂O, Fuchen Chemistry), and deionized water. All chemicals and materials were purchased from commercially available sources and used without further purification. The zeolite Beta with Al/Si = 1:15, which was used as a silica-alumina source in the synthesis of SSZ-13, was purchased from Changchun Third

Party Pharmaceutical Technology.

2.2 Synthesis of embryonic zeolite seeds

The embryonic seeds were prepared employing the method reported in reference 37 [37]. In a typical synthesis, the initial system with a composition 10TMAD:0.28Al₂O₃:27SiO₂:862H₂O was prepared, where EtOH was produced during TEOS hydrolysis. 0.19 g of Al₂(SO₄)₃·18H₂O was added into a solution containing 8.79 g TMAD (35% aq.) and 8.94 g H₂O under stirring to form a clear solution. Then, 5.00 g of TEOS was added dropwise to obtain a clear single-phase suspension. After stirring for 4 h, the suspension was placed into a Teflon-lined stainless steel autoclave and heated at 100 °C for 12 h. The samples are freeze-dried at -80 °C under vacuum for 24 h. Freeze drying is performed, rather than classical oven drying, to avoid any crystallization at this stage. After freeze-drying, we calcined the product at 350 °C for 6 h. Zeolite seeds are denoted as P_{TMAD}.

2.3 Synthesis of ZSM-34 and SSZ-13 with P_{TMAD} seeds

The synthesis of zeolite ZSM-34 and SSZ-13 with P_{TMAD} seeds were performed using the following starting gel:

ZSM-34: 1SiO₂:0.06Al₂O₃:0.43K₂O:65H₂O; 10 wt.% seeds

SSZ-13: 1SiO₂:0.015Al₂O₃:0.43K₂O:65H₂O; 10 wt.% seeds

The effect of KOH, Al, H₂O, and seed content on the purity of the product and the synthesis time were systematically studied. The seed content (wt.%) was determined

based on the weight of SiO₂ in the starting gel. In a typical synthesis, 2.0 g of Ludox HS-40, 0.65 g of KOH, 0.04 g of aluminum, and 14 g of H₂O were mixed and stirred to obtain a homogeneous gel, then 0.08 g of P_{TMAD} was added to the above gel and continually stirred for 1 h. The solution was transferred into a Teflon-lined autoclave and hydrothermally treated at 160 °C for 5 days. The final product was collected by vacuum filtration, washed thoroughly with deionized water until pH 7, and dried at 60 °C overnight.

2.4 Synthesis of reference ZSM-34 and SSZ-13 samples

Highly crystalline zeolite samples were used (1) to validate the effect of P_{TMAD} seeds, and (2) to determine relative crystallinity during crystal growth kinetics studies. The ZSM-34 zeolite with the highest crystallinity obtained according to the procedure reported in Section 2.3 was used as a reference material (Run 14). The SSZ-13 reference material was prepared from interzeolite conversion of zeolite Beta following the procedure reported in reference 32 [32]. In a typical synthesis, TMAD solution with the following molar composition 1SiO₂:0.05Al₂O₃:0.18K₂O:0.31TMAD:30H₂O was prepared. Then, 1.7 g zeolite beta was added (solid/liquid weight ratio of 0.14). The mixture was stirred for 2 h at room temperature and then hydrothermally treated at 150 °C for 24 h. After that, the solid product was collected by vacuum filtration and washed thoroughly with deionized water until a near-neutral pH and then dried overnight at 60 °C.

2.5 Crystal growth kinetics studies

The crystal growth kinetics of the respective zeolites were monitored using XRD analysis. The relative crystallinity of the samples at different crystallization stages was determined by the I_{100} peak area. For instance, the growth kinetics of SSZ-13 was determined by the peak area at 9.4° Two Theta, while the one of ZSM-34 by the peak area at 7.6° Two Theta.

2.6 Characterization

All materials were characterized by Powder X-ray diffraction (PXRD) analysis using a PANalytical B.V. Empyrean powder diffractometer with Cu K_α radiation ($\lambda = 1.5418 \text{ \AA}$) operating at 40 kV and 40 mA. XRD diffraction analysis was used to study the zeolite crystal growth kinetics. Thermogravimetric analysis (TGA) was performed on a SHIMADZU DTG-60 thermal analyzer system. Approximately 10 mg of each sample was introduced in an alumina crucible and loaded in the analyzer chamber. The samples were heated from 30 to 700 °C with a heating ramp of $10 \text{ }^\circ\text{C}\cdot\text{min}^{-1}$ under air (flow rate: $40 \text{ mL}\cdot\text{min}^{-1}$). Scanning electron microscopy (SEM) micrographs were taken on a JEOL JSM7400F microscope operated at 3–10 keV and 10 μA . Transmission electron microscopy (TEM) analysis was performed on a JEM-2100F. The model used for XPS testing is LabRAM HR Evolution, with an excitation light source of 325nm. Prior to the measurement, a diluted colloidal suspension of the

sample was sonicated for 5 min and then dropped on a carbon-film-covered 300-mesh copper electron microscope grids and dried. Energy Dispersive X-Ray Fluorescence Spectrometer (EDX) operated under TEM (JEM-2100F) was used for elemental analysis of the samples. Nitrogen physisorption analyses was performed with a Quantachrome Autosorb-IQ analyzer with ultra-high-purity nitrogen gas (99.999% purity) at 77 K. The calcined samples were analyzed after degassing at 300 °C overnight. The P_{TMAD} test was conducted using instrument ASAP 2020 V4.00 (V4.00G) with argon gas at 87.29 K, and the degassing temperature of 150 °C for 7 h. The specific surface areas (S_{BET}) were obtained using the Brunauer-Emmett-Teller (BET) equation. Based on the Harkins-Jura equation, the microporous volume (V_{mic} , $\text{cm}^3 \text{g}^{-1}$) was obtained from the t-plot.

3.0 Results and Discussion

3.1 Physicochemical properties of P_{TMAD} seeds

In previous studies [37, 38], we have shown that the EZ, are X-ray amorphous, although they possessed some elements of zeolite structure. Similarly, the XRD pattern of precursor P_{TMAD} (Figure S1) does not reveal the presence of a crystalline phase. The TEM analysis (Figure S2) shows that the precursor is composed of sub-nanometer particles with random morphology. The TGA profile of P_{TMAD} (Figure S3) indicates a total weight loss of 11.3 wt.%. Major weight loss (~50% of total weight loss) below 250 °C, coupled with an endothermic peak, is related to the release of

physisorbed water. The exothermic peak at 400–600 °C indicates the combustion of TMAD. Compared to the crystalline TMAD-SSZ-13 zeolite [32], the TMAD in P_{TMAD} was released at a much lower temperature thanks to the more open structure. The amount of occluded TMAD is quite limited (4.9 wt.%), far lower than the amount (~16 wt.%) in the crystalline zeolite [32]. The argon adsorption-desorption analysis of P_{TMAD} sample measured at 87.29K showed a type IV isotherm (Figure S4) with a sharp nitrogen absorption at low pressure ($P/P_0 < 0.2$), which is a characteristic of microporous materials. The surface area S_{BET} of P_{TMAD} , calculated by the Brunauer-Emmett-Teller (BET) equation is $653 \text{ m}^2 \text{ g}^{-1}$, whereas the micropore volume (V_{mic}) is $0.24 \text{ cm}^3 \text{ g}^{-1}$ according to t -plot analysis. The peak positions of the Raman spectrum of P_{TMAD} at 333, 465 and 474 cm^{-1} prove the existence of 4-ring and 6-ring (Figure S5).

TMAD is typically used to direct the synthesis of zeolite SSZ-13 [32] and SSZ-24 [39]. However, the TMAD templated methods are expensive, non-environmental friendly, and require additional treatment steps after the synthesis. In comparison, the zeolite seeded approach is more attractive since it can significantly reduce and even avoid the use of a template, making the zeolite synthesis more economic and environmentally friendly. EZs seeds can extend these advantages further since they can be synthesized under ambient temperature. Herein, we employed the zeolite precursor (P_{TMAD}), which contains embryonic zeolites units, as seeds. Our study showed that in the presence of P_{TMAD} seeds, different zeolite materials can be obtained by varying the Al/Si ratio in the system, i.e., SSZ-13 at $\text{Al/Si} \leq 0.1$, ZSM-34 at $0.1 \leq$

Al/Si \leq 0.2, and LTL at Al/Si = 0.2. Only LTL-type zeolite is formed when the EZ seeds are not used in the synthesis (Run 5, non-seeded). These results reveal the importance of P_{TMAD} seeds in ZSM-34 and SSZ-13 formation.

3.2 Synthesis of ZSM-34

The experimental conditions and results of ZSM-34 synthesis are summarized in Table 1 and the corresponding XRD data is summarized in Figure S6. It was found that besides adding seeds, the potassium and aluminum content are important factors in synthesizing SSZ-34. Pure LTL was obtained at KOH / SiO₂ \geq 0.90 (Run s1, Table s1), while a mixture of ZSM-34 and zeolite L, or ZSM-34 and SSZ-13 appeared at 0.89 \geq KOH / SiO₂ \geq 0.86 (Run s2 to s6, Table s1). And the corresponding XRD data is summarized in Figure S7. Using a gel with KOH / SiO₂ = 0.86 and lower aluminum content (Al / SiO₂ = 0.12) resulted in pure ZSM-34 (Run 1 to 3), and the solid yield is more than 60.5%. With 2.5 wt.% of P_{TMAD} seed, a highly crystalline ZSM-34 was obtained after 5 days of synthesis (Run 3, and 6 to 8). More importantly, the yield of over 55% (run 7-8) is much higher than that of ordinary seed assisted synthesis (27%) [25], demonstrating the effectiveness of using embryonic zeolite as seeds.

Table 1. ZSM-34 synthesis conditions, phase content, and crystallinity.

Synthesis conditions ^a	Product(s)
-----------------------------------	------------

Run	Seeds /wt.%	Seeds type	KOH /SiO ₂	Al /SiO ₂	H ₂ O /SiO ₂	Time /day	Phase (s)	Crystallinity /%	Solid yields/% ^c
1	10	P _{TMAD}	0.86	0.12	65	5	ZSM-34	99	64.1
2	5	P _{TMAD}	0.86	0.12	65	5	ZSM-34	99	62.6
3	2.5	P _{TMAD}	0.86	0.12	65	5	ZSM-34	99	60.5
4	5	ZSM-34	0.86	0.12	65	10	ZSM-34	45	26.2
5 ^b	0	-	0.86	0.12	65	5	LTL	50	72.4
6	2.5	P _{TMAD}	0.86	0.12	65	1	ZSM-34	10	32.2
7	2.5	P _{TMAD}	0.86	0.12	65	3	ZSM-34	50	55.3
8	2.5	P _{TMAD}	0.86	0.12	65	7	ZSM-34	100	61.0

^a All synthesis were performed at 160 °C; ^b TMAD / SiO₂ = 0.5

^c Solid yields (%) = Products after calcination (g) / (SiO₂ of raw material (g)+ seeds (g)) × 100%.

In order to verify the seeding role of P_{TMAD}, we have performed comparative studies with ZSM-34 seed-containing (Run 4) and seed-free (Run 5) systems. In the presence of ZSM-34 seeds (Run 4), compared to using EZ seeds, the product remained amorphous on the 5th day (Figure S8), ZSM-34 of 45% crystallinity (Figure S9a) and bundle-like aggregated crystals (Figure S9b) was formed after 10 days of synthesis. In the absence of seeds (Run 5), the same synthesis system produced zeolite LTL. Therefore, the P_{TMAD} embryonic zeolite seed plays a crucial role in the synthesis of zeolite ZSM-34.

The physicochemical properties of ZSM-34 were studied on a highly crystalline sample (Run 3, Table 1). TG/DTA analysis can provide useful information on the species occluded in zeolite volume and the interaction between the organic template and zeolite framework. The highly crystalline ZSM-34 zeolite showed a weight loss

of ~8% (Figure 1a) below 200 °C, corresponding to the water's endothermic desorption. The weight loss between 200 and 700 °C was about 4 wt.%, attributed to the TMAD combustion, demonstrating the substantial reduction of the OSDA used with respect to conventional OSDA-promoted zeolite synthesis. The content of template agent is much lower than the amount of hexamethylenediamine templates used in traditional hydrothermal synthesis (17.2 wt.%) [22]. The Al/Si ratio of zeolite ZSM-34 was 0.26, according to EDX analysis. This is the lowest silica-alumina ratio reported for ZSM-34 materials [12, 24], which is another benefit of the EZ seed-promoted zeolite crystallization. The nitrogen adsorption-desorption analysis of the ZSM-34 sample measured at 77 K presents the typical of microporous materials steep uptake at low relative pressure (Figure 1b). The S_{BET} and V_{mic} of 348 m² g⁻¹ and 0.14 cm³ g⁻¹ are in line with the values reported in the literature [24], indicating the ZSM-34 obtained in the present work is highly crystalline and comparable to the material obtained from an OSDA-containing system. The pore size distribution curve of the ZSM-34 shows peaks centered at about 4 nm, representing the existence of mesopores (Figure S10a). The inclination of the isotherm with the partial pressure increase is due to the textural porosity of bundle-like crystals.

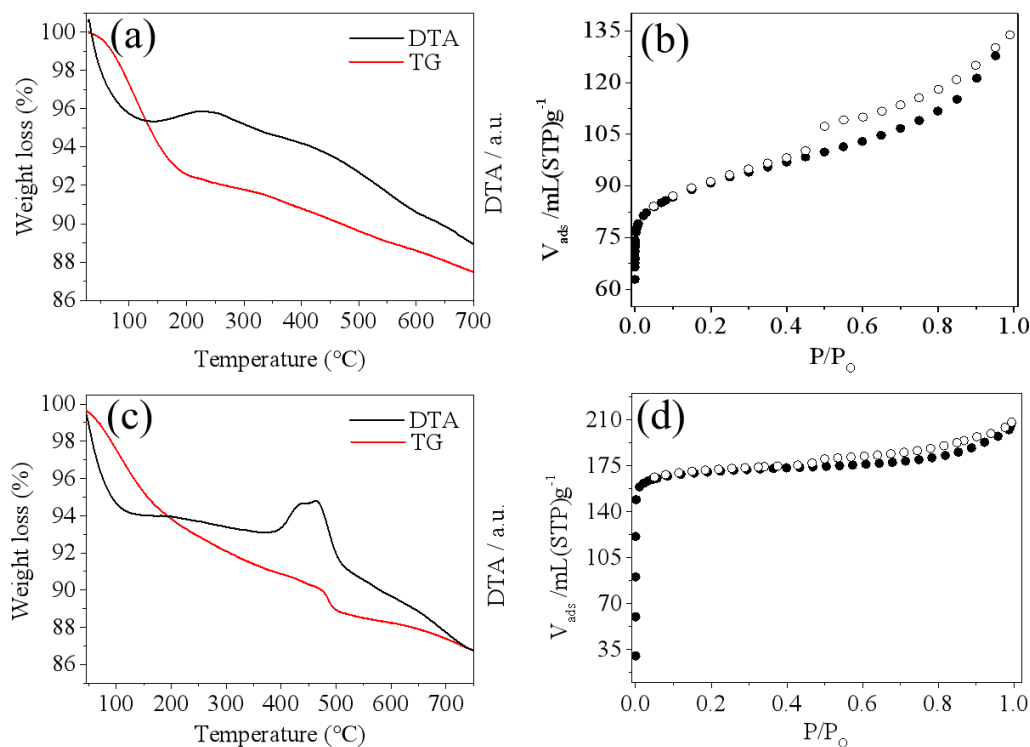


Figure 1. TG/DTA profiles (left) and N₂ adsorption isotherms (right) of zeolite ZSM-34 (a,b) and SSZ-13 (c,d) samples.

3.3 Synthesis of SSZ-13

As mentioned, SSZ-13 can be obtained when $\text{Al} / \text{SiO}_2 \leq 0.10$. The experimental conditions and results are summarized in Table 2 (Run 9 to 18) and the corresponding XRD of the products obtained in Figure S12. When $\text{Al} / \text{SiO}_2 > 0.08$, a mixed SSZ-13 / ZSM-34 solid (Run 9) is formed, while at $0.03 \leq \text{Al} / \text{SiO}_2 \leq 0.8$, pure SSZ-13 (Run 10 to 13) crystallizes, and the crystallinity is the highest when the ratio of Al / SiO_2 is 0.05 (Run 11) and 0.03 (Run 12). It was found that zeolite SSZ-13 with higher crystallinity can also be formed with reduced seed content (5.0 wt.%) when Al / SiO_2 is 0.03 (Run 13), and the solid yield is more than 50.3%. Further decrease of aluminum content ($\text{Al} / \text{SiO}_2 < 0.03$), results in an amorphous product (Run 14) if the

crystallization is limited to 5 days.

In order to clarify the specific role of P_{TMAD} , we have also studied the impact of calcined SSZ-13 seeds and the template (TMAD) without seeding. The template-free SSZ-13 seeds (the seeds size information is shown in Figure S11) yielded pure zeolite SSZ-13 after 15 days of synthesis, which is 5 times longer than using the P_{TMAD} precursor as seeds (Run S7, Table S2). Moreover, the crystallinity (35%) is almost 3 times lower than the product obtained from the P_{TMAD} system (99%, Run 12) under similar conditions. No crystalline material was found after five-days crystallization in the seeds-free system (Run 18). In the latter system containing template (TMADOH), a mixture of ZSM-34 and SSZ-13 was formed (Run S8, Table S2), and the corresponding XRD of the products obtained in Figure S13. Based on this set of experiments, one can conclude that the P_{TMAD} precursor seeds are particularly efficient in synthesizing ZSM-34 and SSZ-13 as the effect goes beyond the simple acceleration of the crystallization reaction.

The physicochemical properties of SSZ-13 were studied on a highly crystalline sample (Run 13, Table 2). TG/DTA analysis shows the amount of TMAD template (350-600 °C) in the SSZ-13 sample is about 4.0 wt.% (Figure 1c), which is far lower than the SSZ-13 prepared by conventional hydrothermal synthesis (20-40 wt.%) [40]. It should be noted that the template content is similar to ZSM-34 obtained with P_{TMAD} seeds. The EDX elemental analysis shows a Al/Si ratio of 0.16. Type I isotherm (Figure 1d) is typical of microporous material is recorded by the N_2 physisorption

analysis. The S_{BET} of $573 \text{ m}^2 \text{ g}^{-1}$ and V_{mic} of $0.25 \text{ cm}^3 \text{ g}^{-1}$ are values closed to a highly crystalline SSZ-13. The pore size distribution curve of the SSZ-13 shows peaks centered at about 4 nm, representing the existence of mesopores (Figure S10b). Furthermore, the solid yield of SSZ-13 reached over 50%, higher than traditional hydrothermal synthesis, but slightly lower than the conversion synthesis from other zeolites [31,32].

Table 2. SSZ-13 synthesis conditions, phase content, and crystallinity.

Run	Synthesis conditions ^a						Product(s)		
	Seeds/ wt. %	Seeds type	KOH/ SiO ₂	Al /SiO ₂	H ₂ O /SiO ₂	Time /day	Phase(s)	Crystallinity / %	Solid yields/% ^b
9	10	P _{TMAD}	0.86	0.10	65	5	ZSM-34+SSZ-13	-	60.3
10	10	P _{TMAD}	0.86	0.08	65	5	SSZ-13	65	53.7
11	10	P _{TMAD}	0.86	0.05	65	5	SSZ-13	98	54.2
12	10	P _{TMAD}	0.86	0.03	65	5	SSZ-13	99	54.0
13	5	P _{TMAD}	0.86	0.03	65	5	SSZ-13	96	50.3
14	5	P _{TMAD}	0.86	0.01	65	5	Amorphous	-	-
15	5	P _{TMAD}	0.86	0.03	65	3	SSZ-13	88	54.1
16	5	P _{TMAD}	0.86	0.03	65	2	Amorphous	-	-
17	5	P _{TMAD}	0.86	0.03	65	1	Amorphous	-	-
18	0	0	0.86	0.03	65	5	Amorphous	-	-

^a All synthesis were performed at 160 °C.

^b Solid yields (%) = Products after calcination (g) / (SiO₂ of raw material (g) + seeds (g)) × 100%.

3.4 Crystallization kinetics of ZSM-34 and SSZ-13 zeolites

To shed more light on the effect of embryonic zeolite seeds, we explored the growth kinetics of ZSM-34 and SSZ-13 in the presence of P_{TMAD} seeds. The evolution of

ZSM-34 phases during growth kinetics studies is monitored by XRD (Figure 2), SEM (Figure 3) and TEM (Figure 4) analyses. A few rod-shaped crystals were observed after 3 days of crystallization (Figure 3 b). The crystallinity increased on the 5th day and reached the maximum on the 7th day (Figure 3 c and d). The solid contains solely uniform crossed rod-shaped agglomerates with 20-40 μm length. The morphology is similar to the previously reported ZSM-34 crystals [24]. Our results show that ZSM-34 can be synthesized using embryonic zeolite seeds at 160 $^{\circ}\text{C}$ for 5 days. This is a dramatic decrease in the synthesis time compared to the traditional synthesis of 17 days [24]. In addition, our method also minimizes the use of OSDA, thus offering a more economical and environmentally friendly way of zeolite synthesis.

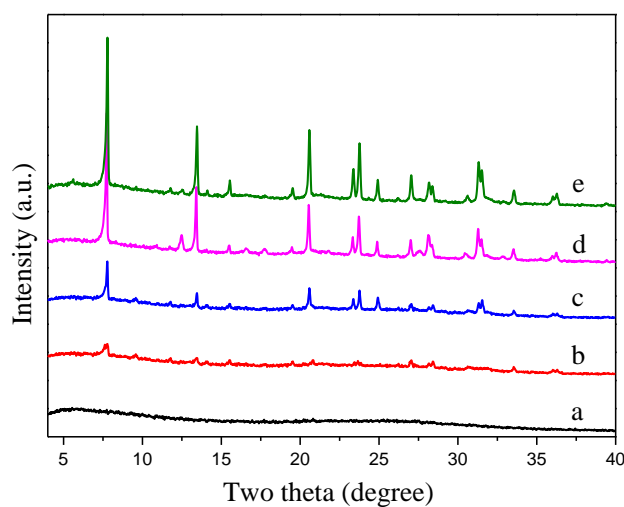


Figure 2. XRD pattern of the growth kinetics of zeolite ZSM-34. (a) 1, (b) 1.5, (c) 3, (d) 5 and (e) 7 days of synthesis.

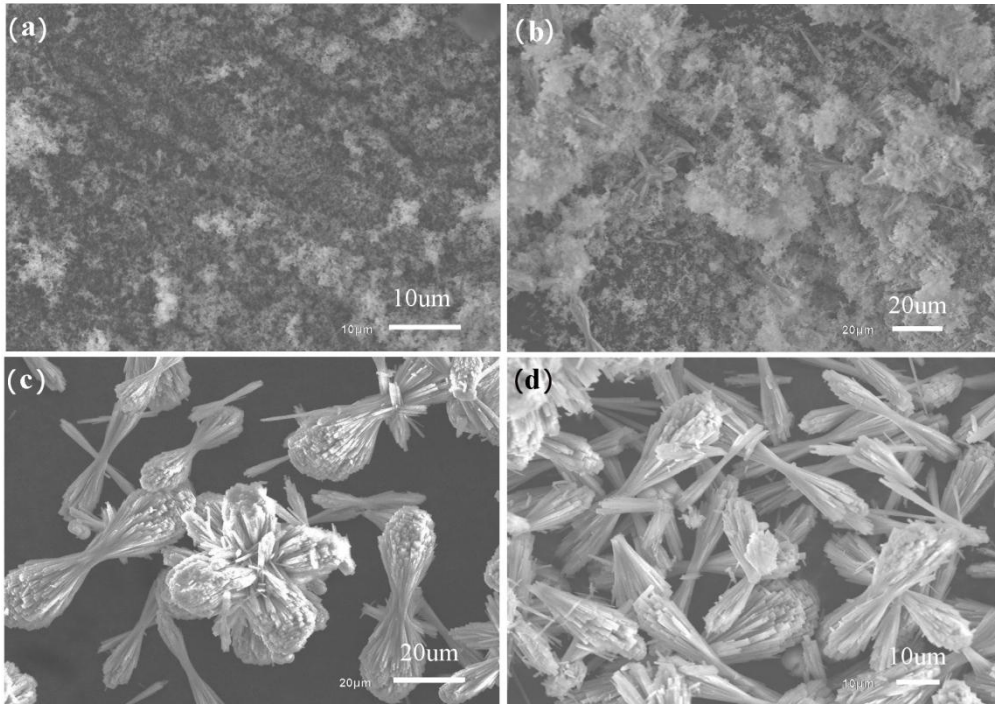


Figure 3. SEM image of zeolite ZSM-34 after (a) 1, (b) 3, (c) 5 and (d) 7 days of synthesis.

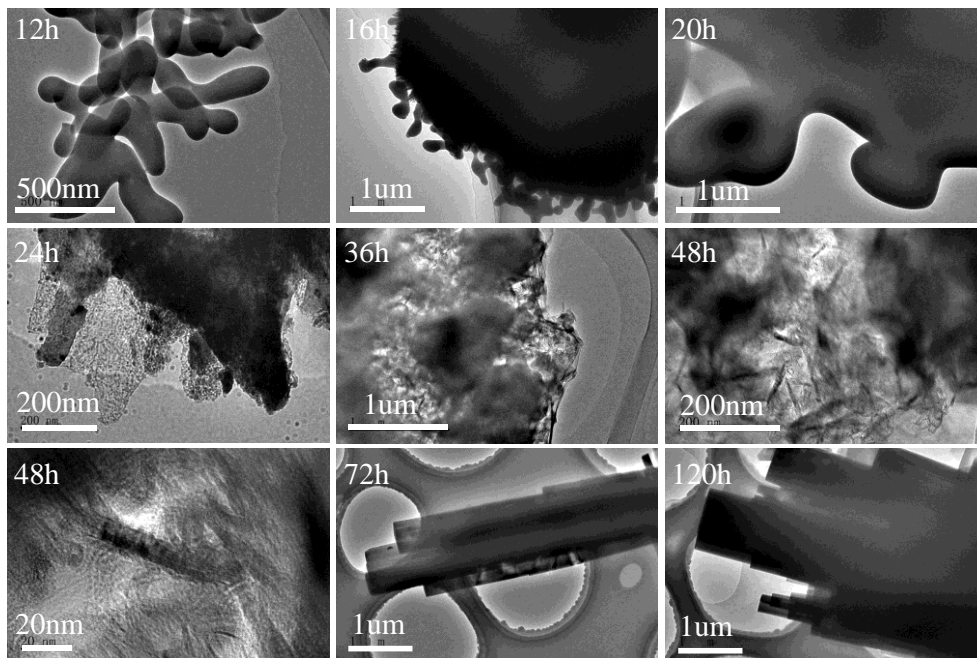


Figure 4. Representative TEM micrographs showing different stages of ZSM-34 crystallization.

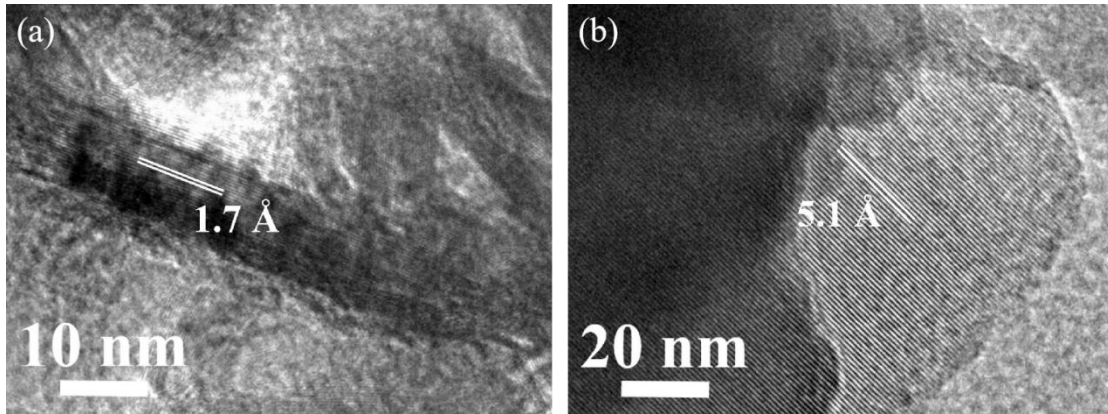


Figure 5. High resolution TEM study of ZSM-34 gel after 48 h of synthesis.

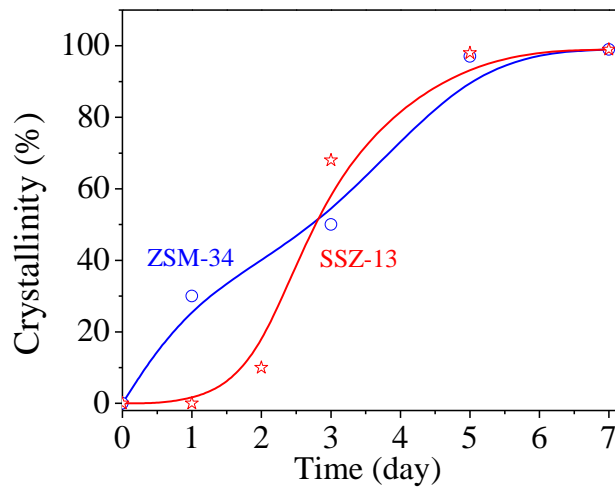


Figure 6. The crystallization curves of zeolite SSZ-13 (red) and ZSM-34 (blue).

We have also explored the early stage (12 h) of ZSM-34 growth (Figure 4), and found that worm-like gel particles are formed. Further they agglomerate into larger particles during the first 16–20 h and eventually transform into needle-like particles after 36 h. At 48 hours, zeolite crystals with a defined morphology and well-established lattice planes can be observed (Figure 5). Figure 5 a–c shows the projections of the framework structure of ZSM-34 along [102] and [101], respectively.

High magnification on the images (inset of Figure 5 a–c) confirmed the lattice spaces of ERI / OFF topologies in ZSM-34 sample.

By referring to the main XRD peak area of reference samples (7.5° in ZSM-34 pattern and 9.3° in SSZ-13 pattern), the crystallization curves for ZSM-34 and SSZ-13 are plotted as shown in Figure 6. The induction period is missing in the case of ZSM-34. After one day of crystallization, the product exhibits 30% crystallinity (Figure 6 blue). The rapid crystallization suggests that the embryonic seeds are extremely efficient in the case of ZSM-34. Also, the higher alkalinity of the initial system contributes to the rapid zeolite formation. Crystallization is completed after 5 days of synthesis for systems.

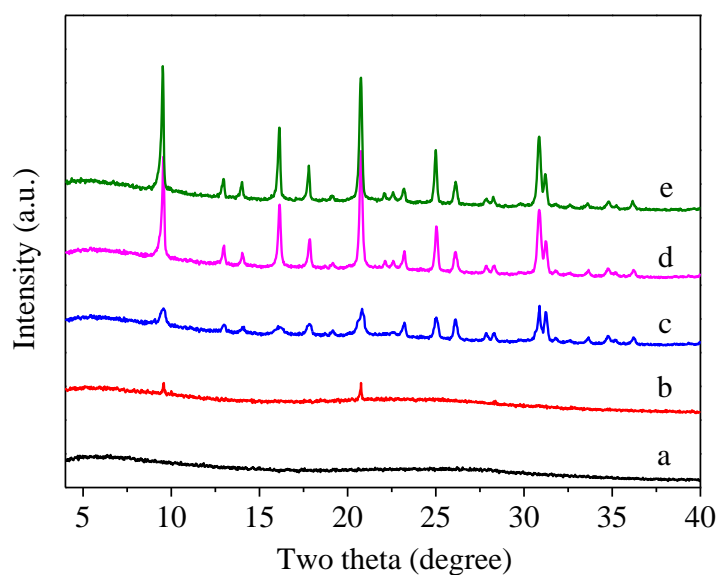


Figure 7. XRD patterns showing the growth kinetics of zeolite SSZ-13 after (a) 1, (b) 2, (c) 2.5, (d) 3 and (e) 5 days of crystallization.

Figures 7 and 8 show the XRD patterns and SEM images collected during the crystal growth kinetics analysis of SSZ-13. Similar to ZSM-34, no crystalline phase is

detected in the first 2 days of synthesis. SSZ-13 crystal phase is observed on the 3rd day with considerably high crystallinity. The crystallization of SSZ-13 features the typical S-type growth curves with an induction period and a steep growth after the second day of synthesis (Figure 6 red). However, a careful inspection under SEM indicates the presence of amorphous particles, which signifies that crystallization is ongoing. Complete crystallization is achieved on the fifth day with the disappearance of amorphous particles. Isometric crystals with distorted cubic shape and sizes of 7–10 μm are observed by SEM.

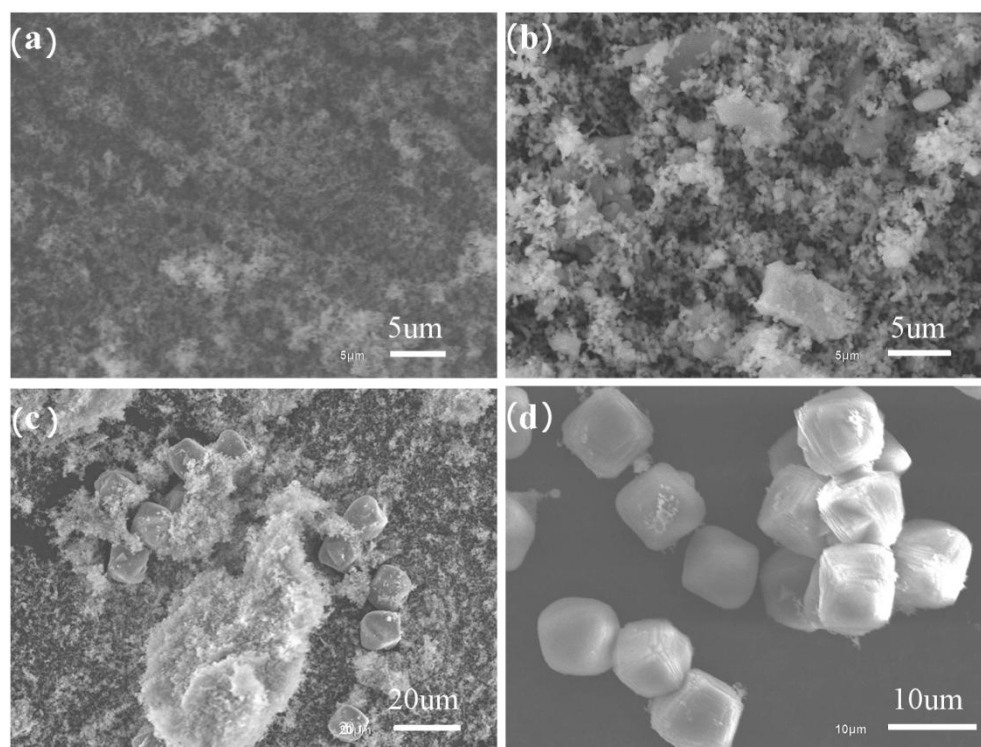

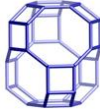







Figure 8. SEM images of zeolite SSZ-13 after (a) 1, (b) 2, (c) 3 and (d) 5 days of crystallization.

3.5 Mechanisms of zeolite formation

Table 3 summarizes the type of frameworks and structure building units in SSZ-13 (CHA) and ZSM-34 (OFF/ERI). Chabazite mineral has commonly been found associated with Offretite (OFF) and Erionite (ERI) in natural deposits [41]. All these structures consisted of the double 6-membered ring (*d6r*) and larger composite units built up of 4- and 6-membered rings. Hence, it is not surprising that the formation of these two zeolites is promoted by one type of seeds. Consequently, the Al content in the initial system plays a crucial role in determining the crystallization route leading to the *cha* cage for SSZ-13 or *can/gme* cage for ZSM-34.

Table 3. The topology and building units of SSZ-13 and ZSM-34.

Zeolite	Topology	Composite building units		
SSZ-13	CHA			
		<i>d6r</i>	<i>cha</i>	
ZSM-34	OFF			
		<i>d6r</i>	<i>can</i>	<i>gme</i>
	ERI			
		<i>d6r</i>	<i>can</i>	

4.0 Conclusion

The present work shows that using embryonic zeolite seeds, generated with TMAD template, is an environmentally benign way to synthesize ZSM-34 and SSZ-

13 crystallization. The method's efficiency is demonstrated by the relatively rapid synthesis of highly pure ZSM-34 and SSZ-13 products. The use of EZ seeds results in a massive reduction in the OSDA used, and more importantly, no hydrothermal treatment is required for seed production. Compared with the conventional crystalline zeolite seeds, the preparation of EZ precursor seeds is more convenient. It involves fewer preparations steps, and the energy consumption is low since the hydrothermal crystallization and washing steps are skipped. All these particularities can bring substantial economic advantages in respect to conventional seeded synthesis. Moreover, the high price of high silica zeolites is mostly due to the expensive OSDA traditionally used in the synthesis. The method established in the present study can bring substantial advantages to the mass production of industrially important zeolites.

Acknowledgments

The ZeoMat Group acknowledges the starting grant provided by QIBEBT, the support provided by the Shandong Energy Institute, and the Nature Science Foundation of Shandong Province. VV, SQ, and QF acknowledge the collaboration under the Sino-French International Research Network (IRN) “Zeolites”.

References

[1] Corma, A. From microporous to mesoporous molecular sieve materials and their use in catalysis. *Chem. Rev.* **1997**, *97*, 2373-2420.

- [2] Davis, M. E. Ordered porous materials for emerging applications. *Nature*. **2002**,*417*, 813-821.
- [3] Cundy, C. S.; Cox, P. A. The hydrothermal synthesis of zeolites: history and development from the earliest days to the present time. *Chem. Rev.* **2003**, *103*, 663-702.
- [4] International Zeolite Association Web site: <http://www.iza-on-line.org/>.
- [5] Lee, H.; Zones, S. I.; Davis, M. E. A combustion-free methodology for synthesizing zeolites and zeolite-like materials. *Nature.*, **2003**, *425*, 385-388.
- [6] Freyhardt, C. C.; Tsapatsis, M.; Lobo, R. F.; Balkus, K. J.; Davis, M. E. A high-silica zeolite with a 14-tetrahedral-atom pore opening. *Nature*. **1996**,*381*, 295-298.
- [7] Lee, H.; Zones, S. I.; Davis, M. E. Zeolite synthesis using degradable structure-directing agents and pore-filling agents. *J. Phys. Chem. B.* **2005**, *109*, 2187-2191.
- [8] Corma, A.; Díaz-Cabañas, M. J.; Martínez-Triguero, J.; Rey, F.; Rius, J. A large-cavity zeolite with wide pore windows and potential as an oil refining catalyst. *Nature*. **2002**, *418*, 514-517.
- [9] Lok, B. M.; Cannan, T.; Messina, C. A. The role of organic molecules in molecular sieve synthesis. *Zeolites*. **1983**, *3*, 282-291.
- [10] Chen, Z.; Li, S.; Yan, Y. Synthesis of template-free zeolite nanocrystals by reverse microemulsion– microwave method. *Chem. Mater.* **2005**, *17*, 2262-2266.
- [11] Bayati, B.; Babaluo, A. A.; Karimi, R. Hydrothermal synthesis of nanostructure NaA zeolite: The effect of synthesis parameters on zeolite seed size and crystallinity. *J.*

Eur. Ceram. Soc. **2008**, *28*, 2653-2657.

[12] Wang, H.; Huang, L.; Holmberg, B. A.; Yan, Y. Nanostructured zeolite 4A molecular sieving air separation membranes. *Chem. Commun.* **2002**, *16*, 1708-1709.

[13] Wang, H.; Holmberg, B. A.; Yan, Y. Synthesis of template-free zeolite nanocrystals by using in situ thermoreversible polymer hydrogels. *J. Am. Chem. Soc.* **2003**, *125*, 9928-9929.

[14] Jhung, S. H.; Chang, J. S.; Park, S. E.; Forster, P. M.; Férey, G.; Cheetham, A. K. Template-free synthesis of the nanoporous nickel phosphate VSB-5 under microwave irradiation. *Chem. Mater.* **2004**, *16*, 1394-1396.

[15] Occelli, M. L.; Innes, R. A.; Pollack, S. S.; Sanders, J. V. Quaternary ammonium cation effects on the crystallization of offretite—erionite type zeolites: Part 1. Synthesis and catalytic properties. *Zeolites.* **1987**, *7*, 265-271.

[16] Inui, T.; Morinaga, N.; Takegami, Y. Rapid synthesis of zeolite catalysts for methanol to olefin conversion by the precursor heating method. *Appl. Catal.* **1983**, *8*, 187-197.

[17] Bessell, S. Investigation of bifunctional zeolite supported cobalt Fischer-Tropsch catalysts. *Appl. Catal A-Gen.* **1995**, *126*, 235-244.

[18] Fan, Z.; Peng, T.; Zhongmin, L.; Guangyu, L.; CHANG, F.; Jinzhe, L. Synthesis of ZSM-34 and its catalytic properties in methanol-to-olefins reaction. *Chinese. J. Catal.* **2007**, *28*, 817-822.

[19] Wei, Y.; Zhang, D.; Liu, Z.; Su, B. L. Highly efficient catalytic conversion of

chloromethane to light olefins over HSAPO-34 as studied by catalytic testing and in situ FTIR. *J. Catal.* **2006**, *238*, 46-57.

[20] Bjørgen, M.; Svelle, S.; Joensen, F.; Nerlov, J.; Kolboe, S.; Bonino, F.; Palumbo, L.; Bordiga, S.; Olsbye, U. Conversion of methanol to hydrocarbons over zeolite H-ZSM-5: On the origin of the olefinic species. *J. Catal.* **2007**, *249*, 195-207.

[21] Xu, T.; Song, H.; Deng, W.; Zhang, Q.; Wang, Y. Catalytic conversion of methyl chloride to lower olefins over modified H-ZSM-34. *Chinese. J. Catal.* **2013**, *34*, 2047-2056.

[22] Vartuli, J. C.; Kennedy, G. J.; Yoon, B. A.; Malek, A. Zeolite syntheses using diamines: evidence for in situ directing agent modification. *Micropor. Mesopor. Mat.* **2000**, *38*, 247-254.

[23] Wu, Z.; Song, J.; Ji, Y.; Ren, L.; Xiao, F. S. Organic template-free synthesis of ZSM-34 zeolite from an assistance of zeolite L seeds solution. *J. Mater. Chem.* **2008**, *20*, 357-359.

[24] Zhang, L.; Yang, C.; Meng, X.; Xie, B.; Wang, L.; Ren, L.; Xiao, F. S. Organotemplate-free syntheses of ZSM-34 zeolite and its heteroatom-substituted analogues with good catalytic performance. *Chem. Mater.* **2010**, *22*, 3099-3107.

[25] Yang, C.; Ren, L.; Zhang, H.; Zhu, L.; Wang, L.; Meng, X.; Xiao, F. S. Organotemplate-free and seed-directed synthesis of ZSM-34 zeolite with good performance in methanol-to-olefins. *J. Mater. Chem.* **2012**, *22*, 12238-12245.

[26] Zones, S. I.; Van Nordstrand, R. A. Novel zeolite transformations: the template-

- mediated conversion of Cubic P zeolite to SSZ-13. *Zeolites*. **1988**, 8, 166-174.
- [27] Zones, S. I. Conversion of faujasites to high-silica chabazite SSZ-13 in the presence of N, N, N-trimethyl-1-adamantammonium iodide. *Journal of the Chemical Society, J. Chem. Soc. Faraday Trans.* **1991**, 87, 3709-3716.
- [28] Van Tendeloo, L.; Gobechiya, E.; Breynaert, E.; Martens, J. A.; Kirschhock, C. E. Alkaline cations directing the transformation of FAU zeolites into five different framework types. *Chem. Commun.* **2013**, 49, 11737-11739.
- [29] Goto, I.; Itakura, M.; Shibata, S.; Honda, K.; Ide, Y.; Sadakane, M.; Sano, T. Transformation of LEV-type zeolite into less dense CHA-type zeolite. *Micropor. Mesopor. Mat.* **2012**, 158, 117-122.
- [30] Goel, S.; Zones, S. I.; Iglesia, E. Synthesis of zeolites via interzeolite transformations without organic structure-directing agents. *Chem. Mater.* **2015**, 27, 2056-2066.
- [31] Martín, N.; Moliner, M.; Corma, A. High yield synthesis of high-silica chabazite by combining the role of zeolite precursors and tetraethylammonium: SCR of NO_x. *Chem. Commun.* **2015**, 51, 9965-9968.
- [32] Tang, L.; Haw, K. G.; Zhang, Y.; Fang, Q.; Qiu, S.; Valtchev, V. Fast and efficient synthesis of SSZ-13 by interzeolite conversion of Zeolite Beta and Zeolite L. *Micropor. Mesopor. Mat.* **2019**, 280, 306-314.
- [33] Jorge, M.; Auerbach, S. M.; Monson, P. A. Modeling spontaneous formation of precursor nanoparticles in clear-solution zeolite synthesis. *J. Am. Chem. Soc.* **2005**,

127, 14388-14400.

- [34] Pashkova, V.; Mlekodaj, K.; Klein, P.; Brabec, L.; Zouzelka, R.; Rathousky, J. Mechanochemical pretreatment for efficient solvent-free synthesis of SSZ-13 zeolite. *Chem-Eur. J.* **2019**, *25*, 12068-12073.
- [35] Wu, H.; Guo, C. Solvent-free synthesis of SSZ-13 zeolite through converting ZSM-5 zeolite. *Mater. Lett.* **2022**, *325*, 132858.
- [36] Wang, L.; Zhu, D.; Wang, J.; Cui, W.; Han, J.; Li, B.; Fan, D.; Tian, P.; Liu, Z. Embryonic zeolite-assisted synthesis of SSZ-13 with superior efficiency and their excellent catalytic performance. *J. Mater. Chem. A.* **2021**, *9*, 15238-15245.
- [37] Haw, K. G.; Goupil, J. M.; Gilson, J. P.; Nesterenko, N.; Minoux, D.; Dath, J. P.; Valtchev, V. Embryonic ZSM-5 zeolites: zeolitic materials with superior catalytic activity in 1, 3, 5-triisopropylbenzene dealkylation. *New. J. Chem.* **2016**, *40*, 4307-4313.
- [38] Akouche, M.; Gilson, J. P.; Nesterenko, N.; Moldovan, S.; Chateigner, D.; Siblani, H. E.; Valtchev, V. Synthesis of Embryonic Zeolites with Controlled Physicochemical Properties. *Chem. Mater.* **2020**, *32*, 2123-2132.
- [39] R. A. Van Nordstr, D. S. Santilli and S. I. Zones, ACS Symp. Ser.; Am. Chem. Soc., Washington, DC, **1988**.
- [40] Zebastian, B.; Bjørnar, A.; Karl, P. L. Preparation of high silica chabazite with controllable particle size. *Micropor. Mesopor. Mat.* **2014**, *195*, 294-302.
- [41] Mattioli, M.; Giordani, M.; Arcangeli, P.; Valentini, L.; Boscardin, M.; Pacella,

A.; Ballirano, P. Prismatic to asbestiform offretite from Northern Italy: Occurrence, morphology and crystal-chemistry of a new potentially hazardous zeolite. *Minerals*. **2018**, *8*, 69.